ELSEVIER

Polymer 44 (2003) 1927–1933

polymer

www.elsevier.com/locate/polymer

Understanding of the tensile deformation in HDPE/LDPE blends based on their crystal structure and phase morphology

Q. Fu[a,*], Y. Men[b,*], G. Strobl[b]

[a]*Department of Polymer Science and Materials, State Key Laboratory of Polymer Materials Engineering, Sichuan University, Chengdu 610065, People's Republic of China*
[b]*Fakultät für Physik, Albert-Ludwigs-Universität, Hermann-Herder-Str. 3, D-79104 Freiburg, Germany*

Received 21 August 2002; received in revised form 10 December 2002; accepted 21 December 2002

Abstract

The mechanisms of tensile deformation in high density polyethylene/low density polyethylene (HDPE/LDPE) blends were studied by a video-controlled tensile set-up, combined with dynamic mechanical analysis and small angle X-ray scattering. When quenching from the melt to room temperature, HDPE forms well-organized spherulits with high crystallinity and rigid amorphous layers between lamellae, and LDPE forms irregular aggregates with low crystallinity and mobile amorphous layers between lamellae. A separate lamellar stack-like structure is formed in HDPE/LDPE blends during the quenching. The deformation is affected by both the crystal structure and the phase morphology. Because the semi-crystalline polymers are made up of two interpenetrating networks, one is built up by the entangled fluid part and the other by the crystallites, at low deformations the coupling and coarse slips of the crystalline blocks dominate the mechanical properties, which allows the system to maintain a homogeneous strain distribution in the sample. The assumption of a homogeneous strain distribution can now be further proved by the tensile deformation in HDPE/LDPE blends, which shows two-step processes, with HDPE crystallites being broken down first at imposed strain of 0.4 and then LDPE crystallites being broken later, at an imposed strain of 0.6.

Keywords: Tensile deformation; True stress–strain curve; Homogeneous strain distribution

1. Introduction

High density polyethylene (HDPE) and low density polyethylene (LDPE) are among the most common used plastics and often used as blends for balanced mechanical properties and processability. One important property of polyethylenes plays the major role for their large number of applications, namely mechanical property. It is well established that the mechanical properties of semi-crystalline polymers are closely related to their crystalline morphology. And furthermore, some recent work showed that the mechanical response may be tightly related to the unique blocky substructure of crystalline lamellae [1–4]. We have performed extensive experimental work on the uniaxial drawing of polyethylene (PE) and syndiotactic polypropylene (sPP) and found a general description for the deformation process [5–8]. Along a true stress–strain curve, one always finds critical strains (A, B and C) where the differential compliance and the recovery property change. The critical strains remain constant under the variation of the crystallinity [5], the deformation temperature, the strain rate [6] and the crystalline lamellar thickness [7]. Obviously, the system can easily react upon the external stress in a well defined way. These critical strains were thus related with:

- the onset of isolated slip processes (point A),
- a change into a collective activity of slips (point B), and
- the beginning of fibril formation after a fragmentation of the lamellar crystals (point C).

As a basic consequence of the strain controlled deformation behavior, the system retains a homogeneous strain distribution during deformation [8,9]. This means that the system is generally built up by two interpenetrating networks, being the entangled fluid part and the crystallites,

* Corresponding authors. Address: BASF Aktiengesellschaft, Department of Polymer Physics, Carl Bosch Str., 67056 Ludwigshafen, Germany. Tel.: +49-1794770512; fax: +49-6216092281.
E-mail address: menyongfeng@yahoo.com (Y. Men).

0032-3861/03/$ - see front matter © 2003 Elsevier Science Ltd. All rights reserved.
PII: S0032-3861(02)00940-0

respectively. When the system is deformed, forces are first transmitted by the crystalline network. The deformation of the crystalline network forces the entangled melt to follow its shape which leads to an orientation of the amorphous part. When the deformation is large, the force generated from the entangled amorphous phase may reach a critical value under which the crystalline blocks are no longer stable. The disaggregated blocks then recrystallize along the drawing direction to form fibrils. The fibrils may well include the previous existed amorphous chains. Support of this idea comes from the fact that the crystalline thickness of the finally largely deformed semi-crystalline samples depends only on the drawing temperature. There is no memory back to the original structure [10]. A careful two-dimensional wide angle X-ray scattering (WAXS) analysis showed that the fibrils start to appear at point C [5,11]. It is thus rather clear that the critical strains at A and B represent mainly the property of the crystalline phase, and the amorphous phase comes into play at the critical strain at C. There exists a transition of the deformation mechanisms from block slips to the dominance of network stretching [8,9]. This transition indicates a continuous loose of the homogeneous strain distribution within the system. As a fact, forces generated from the entangled melt depend on the orientation of the amorphous chains according to the stress-optical rule [12]. The orientation of the amorphous chains is tightly related with the entanglement density. The higher the entanglement density is, the higher is the orientation. This has been proven by a work on a set of polyethylenes with different molecular weight [8,13] which shows changes in the critical strain at C as a function of the molecular weight. In the case of low molecular weight polyethylene, the change in point C is understood as a result of the occurrence of the rigid amorphous phase which gives a higher stress value during stretching. Under such a condition, we observed an abrupt decrease in the critical strain C when the mobility of the amorphous phase is reduced. This is proved by both small angle X-ray scattering (SAXS) experiments which show the thinner amorphous layers and by dynamic mechanical analysis (DMA) measurements which reveal the disappearance of the β-process in low molecular weight samples [13].

Blending of linear HDPE and long chain branched LDPE yields a phase separated morphology after suitable crystallization process. Such a system becomes quite interesting for a mechanical study since the unique morphology. In this work, we select a linear HDPE which has a lower critical strain at C ($\varepsilon_H \sim 0.4$) and an LDPE which has a higher critical strain at C ($\varepsilon_H \sim 0.6$) to study the deformation behavior of their blends in the transition range of critical strain C. The aim of this work is twofold: (1) to understand the tensile deformation (critical strain C) of HDPE and LDPE blends, based on the chain mobility in amorphous region and phase morphology; and (2) to further verify the idea of homogeneous strain distribution by using HDPE/LDPE blends. As described in the following sections, we found that for the blending systems in middle range of deformation two transition points show up at the positions of point C for each homopolymer correspondingly. This could be only possible if a homogeneous strain remains within the different phases. We start with an investigation on morphology and chain mobility, and move on to tensile deformation.

2. Experimental section

2.1. Material

The linear HDPE (former Hoechst AG, Frankfurt) with $M_w = 0.58 \times 10^5$ and 79% crystallinity and the LDPE (BASF AG, Ludwigshafen) with 33 branches per 1000 C atoms and 30% crystallinity were used in this study. HDPE/LDPE blends of 90/10, 70/30, 50/50, 30/70, and 10/90 wt% were prepared in a twin screw extruder at a temperature of 200 °C and a screw speed of 100 rpm for 8 min. The blends were then compression-molded into sheets around 0.4 mm thickness at a temperature of 180 °C. The melt sheets were kept at this temperature for 10 min to complete the polymer chain relaxation before they were transferred quickly into room temperature. Samples with the standard 'dog bone' shape were obtained with the aid of a stamp for tensile test. The specimens for differential scanning calorimetry (DSC), SAXS and DMA experiments were also cut from the melt-pressed sheet.

2.2. True stress–true strain measurement

According to the procedure developed by G'Sell [14,15], true stress–strain curves were measured using an INSTRON 4301 machine equipped with a CCD camera which regulated the crosshead speed so that a constant local strain rate in the narrowest part of the specimen was maintained. The neck profile is registered with the aid of the CCD camera. Assuming a constant sample volume during the stretching, the local strain in the center of the neck can be derived from the minimum diameter. The true stress and strain are continuously registered with the aid of the video camera connected to a computer via a frame grabber. Detail description of the video-control tensile set-up can be found else where [5,16].

2.3. Free shrinkage

To further understand the mechanism of tensile deformation of the samples, we carried out free shrinkage experiment. The sample was extended to a predetermined strain with a constant strain rate, the lower clamp is released, and the change in sample width is monitored via a CCD camera in real-time. The free shrinkage experiment leads to a decomposition of the total strain into two parts, a shrinkage part $\varepsilon_{H,s}$ (elastic) and a rest part $\varepsilon_{H,r}$ (plastic).

Changes in the recovery properties can be easily deduced from this measurement.

2.4. Dynamic mechanical measurement

The measurements on the linear dynamic mechanical properties were carried out by using the Solid Analyzer II of Rheometrix. The dimensions of samples are: length 22 mm, width 6 mm, and thickness around 0.4 mm. The measurement was made at a constant frequency of 10 Hz with a constant strain of 0.1%. The temperature dependence of loss factor tan δ was obtained from the measurement running from -40 to 110 °C at a heating rate of 2 °C/min under a nitrogen atmosphere.

2.5. DSC

Samples used for thermal analysis were removed from the center of the melt pressed sheets and weighed between 5 and 7 mg. Each was scanned in a Perkin–Elmer DSC 7 instrument at 20 °C/min from 25 to 165 °C. The crystallinity was calculated from the measured heat of fusion based upon a perfect crystal heat of fusion of 293 J/g [17].

2.6. SAXS

The SAXS experiments were carried out using a conventional Cu Kα X-ray tube and a Kratky compact camera. Scattering data were analyzed calculating the interface distance distribution function $K''(z)$ and deducing the thickness of crystalline and amorphous layers as well as the linear crystallinity. Details on the SAXS data analysis can be found else where [12,18].

2.7. Polarized light microscope

A polarized light microscope was used to observe the morphology of the blends as well as pure HDPE and LDPE. The samples had the same thermal history as that used for tensile test.

3. Results and discussion

3.1. Crystal morphology and chain mobility

It is well established that HDPE/LDPE blends are homogeneous in the melt [19–22]. However, they may either co-crystallize together, or subject to phase separation depending on cooling rate [20]. To get the direct observation of the morphology of HDPE/LDPE blends, we carried out PLM experiment. The selected results are shown in Fig. 1. As is well known, one observes well organized spherulites for pure HDPE, and irregular spherulits or aggregates for LDPE. The crystal morphologies of the blends lay in between, and the average crystal size is decreasing with the

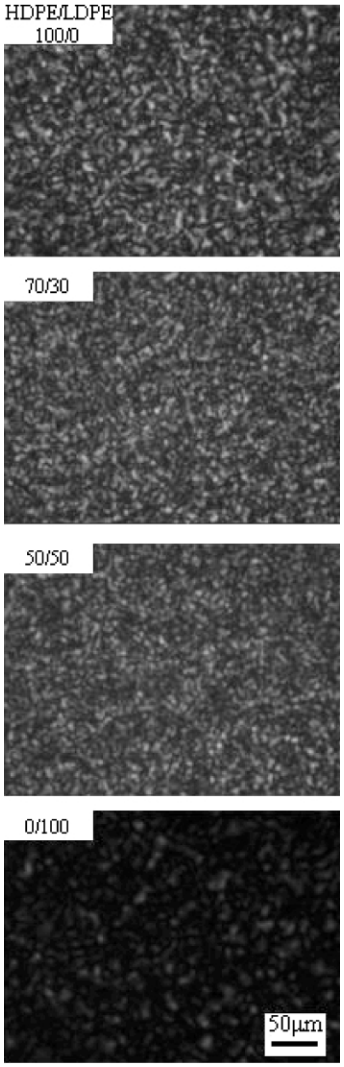

Fig. 1. The PLM micrographs of HDPE and LDPE as well as their blends from which crystalline morphologies may be deduced.

increase in LDPE content. Do HDPE chains co-crystallize together with LDPE or do they form separated lamella stacks during cooling? From PLM images, one cannot get the detailed information about the phase behavior due to the low spacial resolution. Therefore, other experiments are needed. The DSC heating curves of the samples are shown in Fig. 2. Most of the compositions of the blends show two peaks being due to the melting of LDPE and HDPE crystallites, more obvious for 70 and 90 wt% of LDPE. The LDPE peak in the blends is negligible compared with that of the HDPE, if the LDPE content is less than 50 wt%. This is because the LDPE cannot readily crystallize as HDPE does when quenched from the melt to room temperature. As a minor and less crystalline phase, the LDPE crystallizes around the already solidified HDPE to a lesser extent than the pure homo-polymer. The two-phases morphology can be further proved from SAXS data. Fig. 3 shows Lorentz-corrected plots (Is^2 vs. s) of SAXS experiments for the blends as well as for pure HDPE and LDPE. The

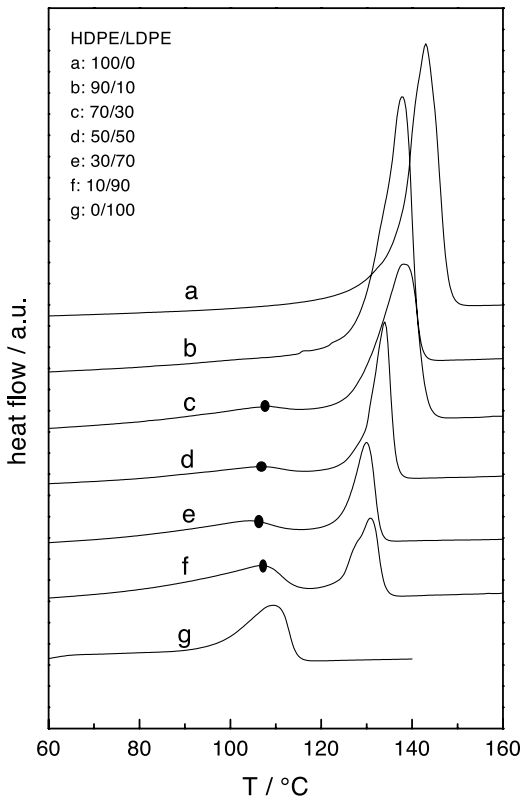

Fig. 2. DSC heating curves of HDPE and LDPE as well as their blends. Heating rate: 20 °C/min. Black dots show the position of peaks due to the melting of LDPE.

characteristic long period peaks for the pure HDPE and LDPE are located at $s \sim 0.04$ and $\sim 0.08\ \mathrm{nm}^{-1}$, respectively. For all the blends, these two peaks are seen which suggests that the components are segregated into separate HDPE and LDPE lamellar stacks in the blends. In case of two peaks, one only can get the long period (L) for each of stack lamellae, but one cannot get the crystalline layer thickness (d_c) and amorphous layer thickness (d_a) by using the interface distance distribution function [18]. For pure HDPE and LDPE, however, d_c and d_a can be obtained. They are 27 nm (L), 22 nm (d_c) and 5 nm (d_a) for HDPE, and 12 nm (L), 3.5 nm (d_c) and 8.5 nm (d_a) for LDPE, respectively, which gives a linear crystallinity ($= d_c/L$) of 81.5% for HDPE and 27.5% for LDPE. The crystallinities obtained by SAXS are consistent with that obtained by DSC from Fig. 2. The much larger amorphous layer thickness of LDPE (8.5 nm) indicates a higher mobility surrounding the crystallites than that surrounding the HDPE crystallites. This can be further proved by DMA data, which are shown in Fig. 4. As examples, the loss factor tan δ as a function of temperature for HDPE, LDPE, blends of compositions HDPE/LDPE of 70/30, and 50/50 are shown. Obviously, there is no β-process for the HDPE, but a clear cut peak around -20 °C for the LDPE. It is believed that the β-process is due to the motion of amorphous phase, thus, the DMA results indicate a rigid, because much confined amorphous layer between the lamellae for HDPE, and a mobile amorphous layer for LDPE. For HDPE/LDPE blends, there exists a sharp decrease in modulus between -20 and 0 °C due to the β-process of LDPE in the blends. For summary of crystal morphological investigations, it can be concluded that the HDPE forms well organized spherulits with a high degree of crystallinity and rigid amorphous layers between the lamellae, and LDPE forms irregular aggregates with low crystallinity and mobile amorphous layers between the lamellae. HDPE and LDPE may be completely miscible in the melt, however, they are segregated into separate lamellar stacks during quenching from the melt to room temperature.

3.2. True stress–strain curves from video-controlled tensile experiment

Having the picture of crystal structure, chain mobility and phase morphology of HDPE/LDPE blends, we go on to understand their tensile behavior. True stress–strain curves were registered under a constant strain rate. In our experiments, the Hencky measure of strain ε_H is used as a

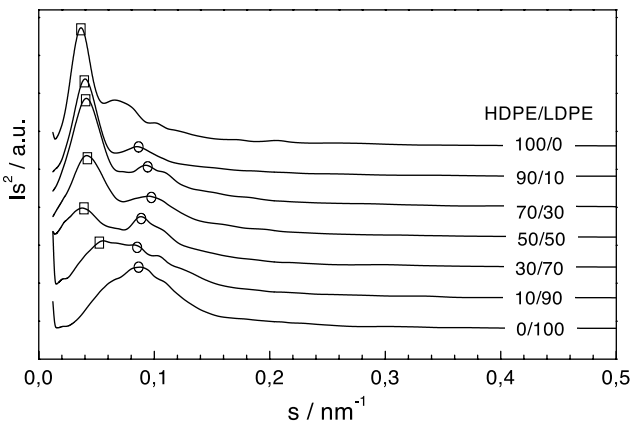

Fig. 3. SAXS result of HDPE and LDPE as well as their blends. Peaks belong to HDPE and LDPE in the curves are marked as hollow squares and hollow circles, respectively.

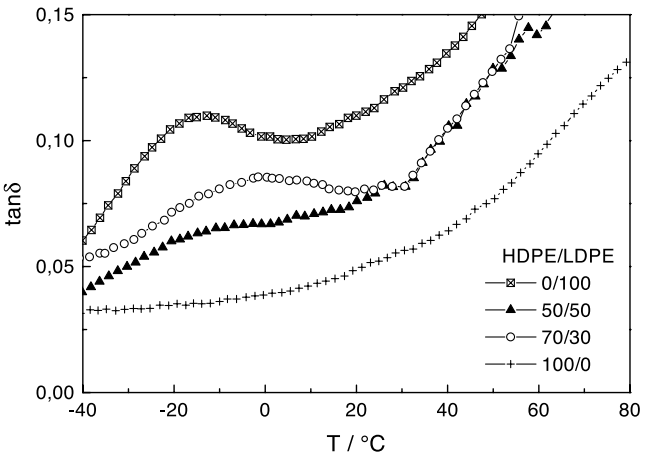

Fig. 4. Mechanical loss factor tan δ of HDPE and LDPE as well as their blends showing different mobility of the amorphous phase. Data derived from DMA measurements.

basic true strain quantity. It is defined as

$$\varepsilon_H = \int_{L_0}^{L} \frac{dL}{L} = \ln \frac{L}{L_0} = \ln(1+\varepsilon) = \ln \lambda \quad (1)$$

where dL is the infinitesimal change of length, L_0 is the original length, L is the current value of the length, ε is the common used nominal strain and λ is the extension ratio. As an example, Fig. 5 shows selected results of stretching runs of samples with different blend composition of HDPE and LDPE. The strain rate was kept constant at $5 \times 10^{-3}\ s^{-1}$. From these true stress–strain curves one always finds that the yield strain (Point B) as defined by the location of maximum curvature remains constant at about $\varepsilon_H \approx 0.12$ whereas the yield stress varies with the overall crystallinity. The enlarged curves at small deformations are also given as an inset in Fig. 5 with which the location of point B can be read out. The present results agrees well with our previous findings that the yield strain is independent of the parameters like crystallinity [5], temperature [6] or molecular weight [8,13].

3.3. Free shrinkage results

To split the tensile deformation into reversible and irreversible parts, we carried out free shrinkage experiments at room temperature. Results are shown in Figs. 6 and 7. For pure HDPE and pure LDPE in which only one kind of stack lamellae exists, at first, both the reversible part $\varepsilon_{H,s}$ and irreversible part $\varepsilon_{H,r}$ increase with the total imposed strain. However, $\varepsilon_{H,s}$ reaches a plateau value at a total stain of 0.4(HDPE) or

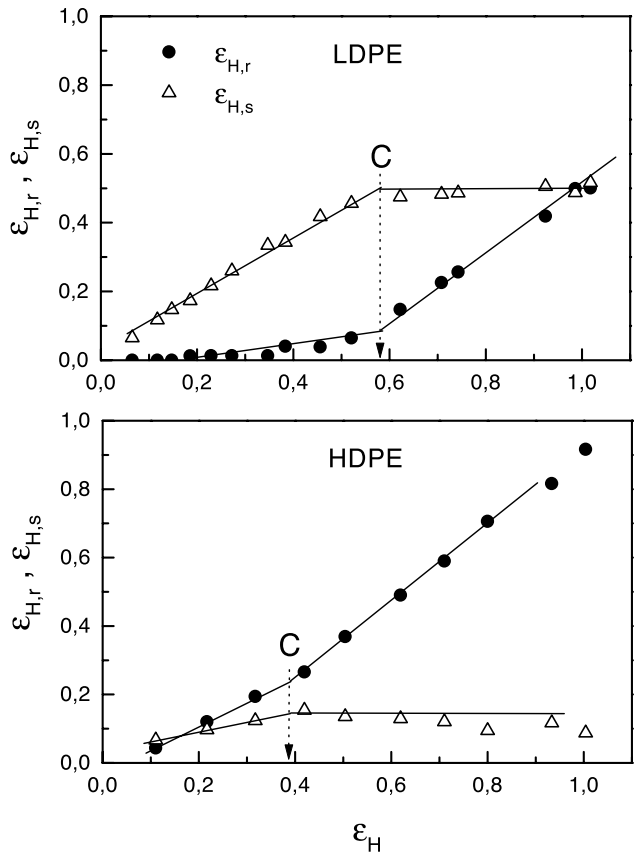

Fig. 6. Partitioning of the total strain into the reversible and irreversible component for HDPE and LDPE (from free shrinkage experiment).

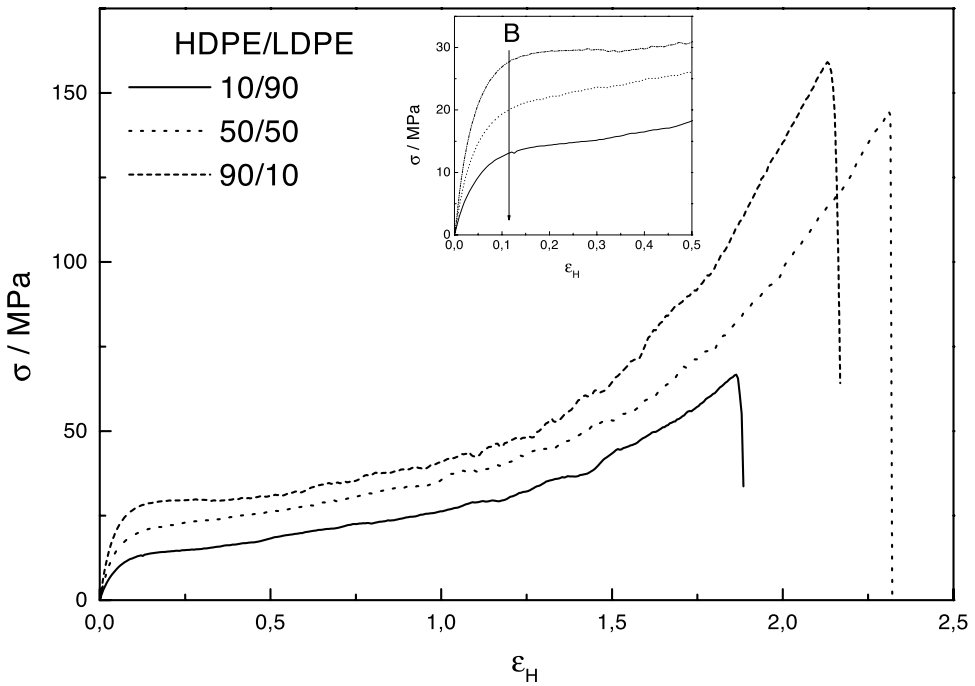

Fig. 5. True stress–strain curve carried out under a constant strain rate of $5 \times 10^{-3}\ s^{-1}$. Inset figure shows the enlarged view at small deformations, the location of point B is marked in the figure.

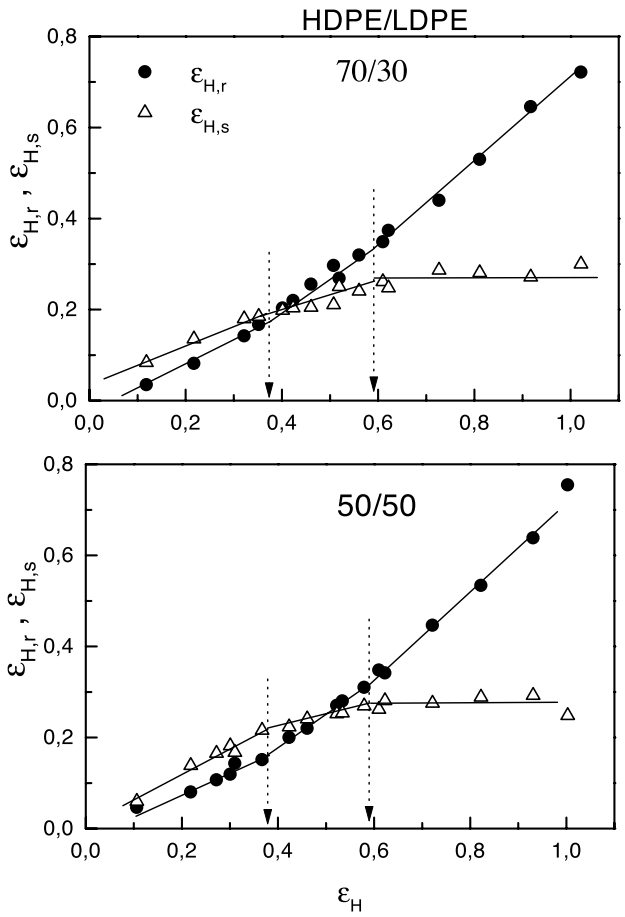

Fig. 7. Partitioning of the total strain into the reversible and irreversible component for HDPE/LDPE blends.

0.6(LDPE); simultaneously, the irreversible part $\varepsilon_{H,r}$ shows a change in differential compliance. The smaller critical stain for HDPE(0.4) compared with LDPE(0.6) is understood as resulting from the much more rigid amorphous layer with high modulus in HDPE, as suggested by SAXS and DMA data [13]. Interesting results come from the HDPE/LDPE blends, which show two kinds of separated stack lamellae. We chose 70/30 and 50/50 blends as examples. As shown in the lower curve of Fig. 7, for both systems, the reversible part $\varepsilon_{H,s}$ and irreversible part $\varepsilon_{H,r}$ are found to increase linearly until the imposed strain reaches a value of 0.4, where both $\varepsilon_{H,s}$ and $\varepsilon_{H,r}$ show a first change of slope. We know from above that 0.4 is the critical strain C for HDPE, so the HDPE crystallites are broken down first in the blends. With further increase in imposed strain, $\varepsilon_{H,s}$ still keep continuously increasing due to the deformation property of LDPE. Until a total strain reaches 0.6, a second change in the slopes is seen. Then $\varepsilon_{H,s}$ reaches a plateau value. Again, we know from above that 0.6 is the critical strain for LDPE, so we believe that LDPE crystallites is also broken down at a total strain of 0.6.

3.4. Homogeneous strain distribution

Over many years it was believed that the stress remains homogeneous when a semi-crystalline polymer is stretched. However, our recent work clearly indicated that not critical stress but critical strain plays a role to determine the tensile deformation of a semi-crystalline polymer. From the finding of a critical strain law governing the deformation process, a homogeneous strain situation is always expected when a semi-crystalline polymer is deformed. We have

$$\varepsilon_H(\text{Cry.}) = \varepsilon_H(\text{Amor.}) = \varepsilon_H \tag{2}$$

where ε_H(Cry.), ε_H(Amor.) and ε_H denote the strain in the crystalline region, amorphous region and for the sample as a whole, respectively. A detailed analysis of the elastic properties for a series of polyethylenes with different crystallinity showed that the above equation holds for strains smaller than point C [8]. Deformation of the crystalline phase is accomplished by block slips which essentially carries the major load before point C is arrived. Amorphous phase would just follow the strain of the crystalline network at first. As stretching increases, the force generated in the entangled melt would reach a critical value under which the crystalline blocks can be disaggregated. This happens first at the strain of point C. Stretching of an entanglement network in semi-crystalline polymers may be well modeled by a Gaussian equation due to the entropic nature of the polymer chains [23,24]. In this way, we have

$$\sigma_{\text{Amor.}} = G\left(\lambda^2 - \frac{1}{\lambda}\right) \tag{3}$$

where $\sigma_{\text{Amor.}}$ is the force generated by the orientation of the amorphous polymer chains, G is the so called network modulus and λ is the extension ratio. The network modulus of HDPE is larger than that of the LDPE's. If the homogeneous strain distribution assumption holds true in HDPE/LDPE blends, at given imposed strain, the stress generated in HDPE should be larger than that in LDPE. So the critical stress is reached first for HDPE at smaller strain ($\varepsilon_H(C) = 0.4$), and at a larger strain for LDPE ($\varepsilon_H(C) = 0.6$). Thus a two-step processes like deformation is expected. This agrees well with the observation in free shrinkage experiments of HDPE/LDPE blends. So homogeneous strain distribution assumption is further verified in a phase separated HDPE/LDPE blends.

4. Conclusions

The mechanism of the tensile deformation in HDPE and LDPE as well as their blends was studied based on true stress–strain measurements obtained via a video-controlled tensile set-up. The chain mobility and crystal morphology have vital effects on critical strain. HDPE has a smaller critical strain ($\varepsilon_H(C) = 0.4$) due to its rigid amorphous, compared with that of LDPE ($\epsilon_H(C) = 0.6$). A two-step

deformation process was observed in tensile experiment of HDPE/LDPE blends, with each step corresponding to the tensile behavior of the each component. This can only be understood if the strain distribution in the sample is homogeneous.

Acknowledgements

We thank Ms Barbara Heck for her help in the SAXS measurements. Support of this work by the Deutsche Forschungsgemeinschaft (Sonderforschungsbereich 428 and Graduiertenkolleg 'Strukturbildung in Makromolekularen Systemen') is gratefully acknowledged. Q.F. would like to express his gratitude to the Alexander von Humboldt-Stiftung, the China National Distinguished Young Investigator Fund and the National Nature Science Foundation of China for their financial support.

References

[1] Gerrits N, Tervoort Y. J Mater Sci 1992;27:1385.
[2] Seguela R, Rietsch F. J Mater Sci 1990;9:46.
[3] Hugel T, Strobl G, Thomann R. Acta Polym 1999;50:214.
[4] Loos J, Thuene PC, Lemstra PJ, Niemantsverdriet JW. Macromolecules 1999;32:8910.
[5] Hiss R, Hobeika S, Lynn C, Strobl G. Macromolecules 1999;32:4390.
[6] Hobeika S, Men Y, Strobl G. Macromolecules 2000;33:1827.
[7] Men Y, Strobl G. J Macromol Sci Phys 2001;B40:775.
[8] Men Y. PhD Thesis. University of Freiburg; 2001.
[9] Men Y, Strobl G. Chin J Polym Sci 2002;20:161.
[10] Balta-Calleja FJ, Peterlin A. J Macromol Sci -Phys 1970;B4:519.
[11] Hobeika S. PhD Thesis. University of Freiburg; 1999.
[12] Strobl G. The physics of polymers. Berlin: Springer; 1997. p. 349.
[13] Fu Q, Men Y, Strobl G. Polymer 2003; in press.
[14] G'Sell C, Jonas J. J Mater Sci 1979;14:583.
[15] G'Sell C, Hiver J, Dahoun A, Souahi A. J Mater Sci 1992;27:5031.
[16] Hiss R. PhD Thesis. University of Freiburg; 1996.
[17] Wunderlich B. Thermal analysis. New York: Academic Press; 1990.
[18] Hauser G, Schmidtke J, Strobl G. Macromolecules 1998;31:6250.
[19] Alamo RG, Londono JD, Mandelkern L, Stehling C, Wignall GD. Macromolecules 1994;27:411.
[20] Wignall GD, Londono JD, Lin JS, Alamo RG, Galante MJ, Mandelkern L. Macromolecules 1995;28:3156.
[21] Bates FS, Wignall GD, Koehler WC. Phys Rev Lett 1985;55:2425.
[22] Bates FS, Dierker SB, Wignall GD. Macromolecules 1986;19:1938.
[23] Haward R, Thackray G. Proc R Soc A 1968;302:453.
[24] Haward R. Macromolecules 1993;26:5860.